Robust and reentrant superconductivity in magic-angle twisted trilayer graphene

Jie Cao,[1,*] Fenghua Qi,[2,*] Yuanyuan Xiang,[1] and Guojun Jin[3,4,†]
[1]*College of Science, Hohai University, Nanjing 210098, China*
[2]*School of Electronic Engineering, Nanjing Xiaozhuang University, Nanjing 211171, China*
[3]*School of Physics Science and Technology, Kunming University, Kunming 650214, China*
[4]*National Laboratory of Solid State Microstructures, Department of Physics, and Collaborative Innovation Center of Advanced Microstructures, Nanjing University, Nanjing 210093, China*

(Received 14 September 2023; revised 18 December 2023; accepted 19 December 2023; published 9 January 2024)

The recent discovery of superconductivity in magic-angle twisted trilayer graphene (MATTG) has sparked significant interest. Here we focus on MATTG, where the low energy flat bands and linearly dispersive Dirac bands coexist and can be decoupled by external fields. Using a continuum model, we examine the low-energy electronic structures and superconductivity for various external fields and small lateral shifts. We find that small lateral shifts play a crucial role by interacting with magnetic fields to increase the density of states in the flat bands, resulting in an anomalous superconducting phenomenon that strengthens with increasing magnetic field strength. Electric displacement fields and sublattice polarization, even though both break the $\mathcal{C}_2\mathcal{M}_h$ symmetry, contribute in opposite ways to the robustness of superconductivity. The interplay of these mechanisms can give rise to reentrant superconductivity under specific parameter settings. Our findings provide insights into the external field-regulated robustness and reentrant superconductivity in the MATTG system.

DOI: 10.1103/PhysRevB.109.035115

I. INTRODUCTION

Superconductivity has been observed in magic-angle twisted bilayer graphene (MATBG) for certain flat-band fillings in recent experiments [1–4]. Theoretically speaking, superconductivity in MATBG arises from the fact that the strength of effective interactions between electrons in the flat bands near Fermi energy is larger than or comparable to the bandwidth of the flat bands. A lot of groups have explored several theoretical models such as unconventional superconductivity driven by strong electron-electron interactions [5–15] and conventional superconductivity mediated by electron-phonon interactions [16–22]. Subsequently, the researches on twisted multilayer graphene systems have made a significant advancement [23–31] due to their potential for tuning the band structures and topology of the flat bands using external fields. In particular, the discovery of superconductivity in magic-angle twisted trilayer graphene (MATTG) has attracted much attention. MATTG and MATBG share identical low-energy flat bands, differing only in twist angle by a factor of $\sqrt{2}$ [32–35], about 1.05° and 1.56° respectively, suggesting a common origin for their superconductivity.

However, experimental measurements indicate that the superconductivity in MATTG is more robust against in-plane magnetic fields than in MATBG [28]. This fact can arise from the subtle differences in the flat band structure. For instance, MATTG possesses both even-parity flat bands and odd-parity Dirac bands, which can be intermixed through external fields. In Fig. 1, we plot the band structure of MATBG (red lines) and MATTG (black lines) in the chiral limit where the interlayer coupling in the AA region is neglected [36]. We can see that the flat bands in MATBG and MATTG exhibit distinct responses to in-plane magnetic fields. In the case of MATTG, an in-plane magnetic field couples the flat bands at the $\overline{K}$ point with the Dirac dispersive bands, resulting in a relatively small overall band transformation in the flat bands. In contrast, for MATBG, the flat bands undergo a significant overall widening under the influence of an in-plane magnetic field, with only the degeneracy maintained at the Γ point. We can potentially explain why superconductivity remains robust in the presence of in-plane magnetic fields in MATTG. Moreover, in the chiral limit, the symmetry of flat bands is efficient and can be used to explain the superconducting phenomena [37]. Therefore, the chiral limit is adopted in this study.

This work focuses on MATTG, where the outer two layers are almost perfectly aligned, and the low energy flat bands and linearly dispersive Dirac bands coexist and can be joined in external fields. We employ a continuum model to compute the low energy electronic structures and the superconductivity for various external fields and small lateral shifts between the two outer layers. Specifically, we find that small lateral shifts, electric displacement fields introduced by gates, and sublattice polarization play distinct roles in determining the behavior of superconductivity in MATTG. Notably, small lateral shifts, although their proper control is currently challenging in experimental settings, have emerged as a crucial factor. The significance stems from its interaction with magnetic fields, which results in an increased density of states (DOS) within the flat bands. With the enhancement of the DOS, the superconducting critical temperature (T_c) exhibits a maximum

*These authors contributed equally to this study.
†Corresponding author: gjin@nju.edu.cn

near the DOS peak, signifying an anomalous superconducting phenomenon that strengthens with higher magnetic field strengths.

On the other hand, the application of the electric electric displacement fields breaks both time-reversal and mirror ($\mathcal{T}\mathcal{M}_h$) and twofold rotation and mirror ($\mathcal{C}_2\mathcal{M}_h$) symmetries, where $\mathcal{M}_h$ takes $z \to -z$ while other two-dimensional mirror symmetries are not considered. This breaking causes energy splitting within Cooper pairs, leading to a decrease in T_c, as outlined in [38]. However, the breaking of $\mathcal{C}_2\mathcal{M}_h$ symmetry does not invariably result in a reduction of T_c, as observed with the inclusion of the sublattice polarization term. Intriguingly, we observe that the presence of the sublattice polarization term enhances the effective interaction strength projected onto the flat bands. Despite the breaking of $\mathcal{C}_2\mathcal{M}_h$ symmetry, this stronger attractive interaction leads to an increase in T_c.

As one can find, Ref. [38] has already made a detailed study of the MATTG system. However, there are still some different treatments can be performed and interesting results can be obtained. For example, in our work, by considering the chiral limit, we find that a small lateral shift of an outer layer is crucial for elucidating the robustness of superconductivity against in-plane magnetic fields. On the other hand, our calculations within the framework of BCS theory make clear the reason for the reentrant superconductivity [28], suggesting the mechanism of superconductivity in MATTG is likely of a conventional nature. Furthermore, the electric displacement field and sublattice polarization, both breaking the $\mathcal{C}_2\mathcal{M}_h$ symmetry, exert opposing influences on the critical temperature T_c, in contrast to the previous claim [38].

The remainder of this paper is structured as follows. In Sec. II, we first briefly review the effective continuum model for MATTG, then the modulation of the in-plane magnetic field and small lateral shift are considered. In Sec. III, we calculate the low-energy band structure under the influence of different external fields and the superconducting transition temperature using the Bardeen-Cooper-Schrieffer (BCS) model. We find that the robustness of superconductivity is strongly correlated with the lateral shift and the sublattice polarization. Finally, we give a suitable discussion and brief conclusions in Sec. IV.

II. MODEL AND FORMULATION

A. Continuum model for MATTG

A single-particle band model of MATTG can be obtained by generalizing the Bistritzer-MacDonald's MATBG model [39]. We construct MATTG by rotating layer 1, layer 2, and layer 3 with angles $\theta/2$, $-\theta/2$, and $\theta/2$, respectively, in a totally overlapping graphene trilayer. In MATTG, the lattice constant is $L = a/2\sin(\theta/2)$, where a is the lattice constant of a graphene monolayer (GML). In momentum space, as shown in Fig. 2(a), the two Dirac points of the rotated graphene layers are separated by $k_\theta = 2k_0\sin(\theta/2)$, where $k_0 = 4\pi/3a$. In the basis $(\psi_1, \psi_2, \psi_3)^{\mathrm{T}}$ where the spinor $\psi_i = (\psi_i^{\mathrm{A}}, \psi_i^{\mathrm{B}})$ and A/B is the sublattice index, the K-valley Hamiltonian is [38]

$$\mathcal{H}_K(\boldsymbol{k}) = \begin{pmatrix} h_{\theta/2}(\boldsymbol{k}) & T(\boldsymbol{r}) & 0 \\ T^\dagger(\boldsymbol{r}) & h_{-\theta/2}(\boldsymbol{k}) & T^\dagger(\boldsymbol{r}) \\ 0 & T(\boldsymbol{r}) & h_{\theta/2}(\boldsymbol{k}) \end{pmatrix}, \qquad (1)$$

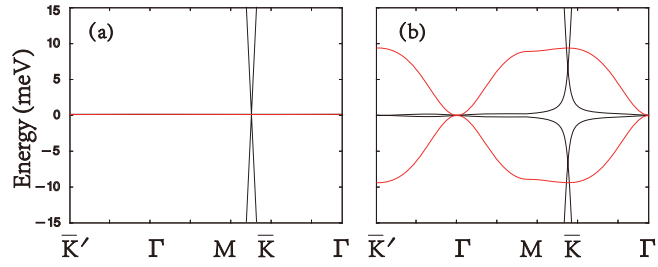

FIG. 1. Energy band structures of MATBG and MATTG, the red lines for the former and black lines for the latter. The in-plane magnetic field is set as (a) $B = 0$, (b) $B = 5$ T.

where $h_\theta(\boldsymbol{k}) = e^{i(\theta/2)\sigma_z}(v_{\mathrm{D}}\boldsymbol{k}\cdot\boldsymbol{\sigma})e^{-i(\theta/2)\sigma_z}$, and v_{D} is the Dirac velocity in an individual GML. $\boldsymbol{\sigma} = (\sigma_x, \sigma_y)$ are the Pauli matrices of psuedospin. The interlayer coupling matrix $T(\boldsymbol{r}) = \sum_{j=1}^{3} T_j e^{-i\boldsymbol{q}_j\cdot\boldsymbol{r}}$, where $T_j = w_{\mathrm{AA}}\sigma_0 + w_{\mathrm{AB}}[\sigma_x\cos(j-1)\phi + \sigma_y\sin(j-1)\phi]$ with $\phi = 2\pi/3$. w_{AA} and w_{AB} are the interlayer hopping parameters in the AAA and ABA(BAB) stacking regions. The three-momentum transfers $\boldsymbol{q}_j$ are $\boldsymbol{q}_1 = k_\theta(0, -1)$, $\boldsymbol{q}_2 = k_\theta(\sqrt{3}/2, 1/2)$, and $\boldsymbol{q}_3 = k_\theta(-\sqrt{3}/2, 1/2)$, as shown in Fig. 2(b). In the chiral limit with $w_{\mathrm{AA}} = 0$ [25], one can eliminate the twists in kinetic terms, i.e., $\boldsymbol{\sigma}_{\pm\theta/2} \to \boldsymbol{\sigma}$ by rotating the spinors. In the following, we focus on the chiral limit if there is no special statement.

B. In-plane magnetic field

The application of an in-plane magnetic field $\boldsymbol{B}_\parallel$ to MATTG as well as to MATBG induces a layer-dependent gauge field $\boldsymbol{A}_l = \boldsymbol{B}_\parallel \times \boldsymbol{z}_l$ [38]. For MATBG, the gauge field shifts the momenta of Dirac electrons in the top and bottom

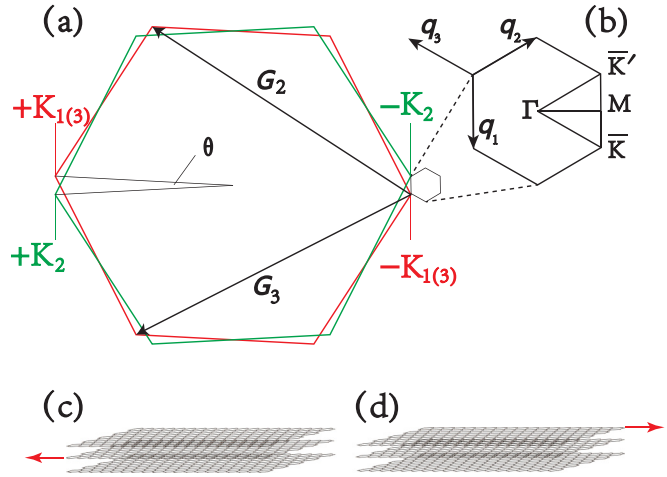

FIG. 2. (a) Brillouin zone folding in the MATTG with a small twist angle θ. The two large hexagons represent the first Brillouin zones (BZs) of the three GMLs distinguished by red (layer 1 and 3) and green (layer 2), with $\pm K_{1(3),2}$ as the valleys in the BZs. (b) The small hexagon is the moiré Brillouin zone (MBZ) of the MATTG, with $\overline{K}$ and $\overline{K}'$ as the valleys in the MBZ. The three $\boldsymbol{q}_j$ are the momentum transfers that correspond to the three interlayer hopping processes. (c) and (d) depict schematically the two kinds of lateral shifts between the intermediate layer and the outer layers.

layers along opposite directions, respectively, so that

$$\mathcal{H}_{\mathrm{K}}^{\mathrm{B}}(\boldsymbol{k}) = \begin{pmatrix} h(\boldsymbol{k}+\boldsymbol{A}/2) & T(\boldsymbol{r}) \\ T^{\dagger}(\boldsymbol{r}) & h(\boldsymbol{k}-\boldsymbol{A}/2) \end{pmatrix}, \tag{2}$$

where $\boldsymbol{A} = (\pi d_0/\Phi_0)(B_y, -B_x)$, d_0 is the average interlayer distance, and Φ_0 denotes the magnetic flux quantum. The point with $z = 0$ is set at the center of the two layers. Since the electrons in the MBZ corners $\overline{K}$ and $\overline{K}'$ are mainly contributed by layer 1 (or 2), the gauge field affects the bands mostly at the corners of the MBZ. As shown in Fig. 1(b), the application of $\boldsymbol{B}_{\parallel}$ causes a broadening of the bandwidth and distortion of the Fermi surface all over the MBZ except the Γ point, therefore leading to a reduction on the superconducting critical temperature T_{c}.

In the MATTG case, however, choosing $z = 0$ in the middle layer, the gauge field only shifts the momenta of electrons in the top and bottom layers. The K-valley Hamiltonian becomes

$$\mathcal{H}_K(\boldsymbol{k}) = \begin{pmatrix} h(\boldsymbol{k}+\boldsymbol{A}) & T(\boldsymbol{r}) & 0 \\ T^{\dagger}(\boldsymbol{r}) & h(\boldsymbol{k}) & T^{\dagger}(\boldsymbol{r}) \\ 0 & T(\boldsymbol{r}) & h(\boldsymbol{k}-\boldsymbol{A}) \end{pmatrix}, \tag{3}$$

with the M_h symmetry breaking since the sign of $\boldsymbol{A}$ is changed by the M_h operation. In Fig. 1(b), the presence of $\boldsymbol{B}_{\parallel}$ only induces a sharp energy shift in the vicinity of the $\overline{K}$ point, while the energy dispersion in most of the BZ is rarely changed. Furthermore, the two valleys can be mapped to each other by the combined $\mathcal{C}_2\mathcal{M}_h$ or $\mathcal{T}\mathcal{M}_h$ symmetry [38]. Therefore, even in the presence of a in-plane magnetic field, there exists a perfect intervalley Fermi surface nesting favorable for the superconducting pairing. One can expect that the superconductivity in MATTG can survive at large values of $\boldsymbol{B}_{\parallel}$.

C. Lateral shift of one outer layer

In MATBG, lateral shift of one layer does not influence the electronic structure since a new AA stack region can always be found as the coordinate origin. A similar case occurs when a lateral shift is applied to the middle layer in MATTG as illustrated in Fig. 2(c). However, relative lateral shift of the two outer layers significantly changes the electronic structure of MATTG [35]. From the symmetry perspective, lateral shift of the top or bottom layer not only breaks the $\mathcal{M}_h$ symmetry but also the $\mathcal{C}_2\mathcal{T}$ symmetry. Consequently, the degeneracy of the flat-band Dirac cone is no longer protected. Moreover, the C_{3v} symmetry is also broken upon applying a lateral shift, leading to a strong anisotropy in the electronic structure.

D. Combined effects on the Hamiltonian

The lateral shifts in realistic MATTG are important, and their influence should be included in the continuum model. To account for such shifts, one may consider a scenario where a lateral shift $\boldsymbol{d}$ affects only the top layer of MATTG as illustrated in Fig. 2(d). As a result, the AA stacking region of the top and middle layers undergoes a perpendicular shift of $\gamma|\boldsymbol{d}|$, where $\gamma = [2\tan(\theta/2)]^{-1}$. However, the AA stacking region of the middle and bottom layers remains unaffected, with the most well-stacked AAA region situated between these two points. This situation is equivalent to leave the middle layer unchanged while shifting the top and bottom layers by $\boldsymbol{d}/2$ and $-\boldsymbol{d}/2$, respectively. The continuum Hamiltonian is then modified as

$$\mathcal{H}_K(\boldsymbol{k}) = \begin{pmatrix} h(\boldsymbol{k}+\boldsymbol{A}) & T'(\boldsymbol{r}, \boldsymbol{d}/2) & 0 \\ T'^{\dagger}(\boldsymbol{r}, \boldsymbol{d}/2) & h(\boldsymbol{k}) & T'^{\dagger}(\boldsymbol{r}, -\boldsymbol{d}/2) \\ 0 & T'(\boldsymbol{r}, -\boldsymbol{d}/2) & h(\boldsymbol{k}-\boldsymbol{A}) \end{pmatrix}, \tag{4}$$

where $T'(\boldsymbol{r}) = \sum_{j=1}^{3} T_j e^{-i\boldsymbol{q}_j\cdot\boldsymbol{r} - i\boldsymbol{G}_j\cdot\boldsymbol{d}/2}$. These lateral shifts preserve $\mathcal{C}_2\mathcal{M}_h$ symmetry, thereby retaining the state degeneracy.

III. FLAT BANDS AND SUPERCONDUCTIVITY UNDER APPLIED-FIELD MODULATIONS

A. Reappearance of super flat bands

In Fig. 3, we plot the calculated band structure under different in-plane magnetic fields in the presence of a lateral shift. When there is no magnetic field, the flat bands and the higher-energy bands are in contact. When an in-plane magnetic field is applied, the degeneracy point between the flat bands and the higher-energy bands is lifted. As the in-plane magnetic field increases, the bands at the $\overline{K}$ point are flattened, until at some magnetic field value, the flat bands become almost widthless. As the magnetic field continues to increase, the flat bands swell again at the $\overline{K}$ point, but, due to the presence of the lateral shift, the flat bands are always separated from the other bands. It is observed that when no in-plane magnetic field or lateral shift is present, the lowest bands always touch the higher-energy bands. However, the coexistence of these two factors leads to the opening of a gap at the touching point.

Neither the in-plane magnetic field nor the lateral shift breaks the chiral symmetry, therefore, one can reshuffle the basis to $(\psi_+^{\mathrm{A}}, \psi_2^{\mathrm{A}}, \psi_-^{\mathrm{A}}, \psi_+^{\mathrm{B}}, \psi_2^{\mathrm{B}}, \psi_-^{\mathrm{B}})^{\mathrm{T}}$ where $\psi_{\pm} = (\psi_1 \pm \psi_3)/\sqrt{2}$. The Hamiltonian in the new basis is

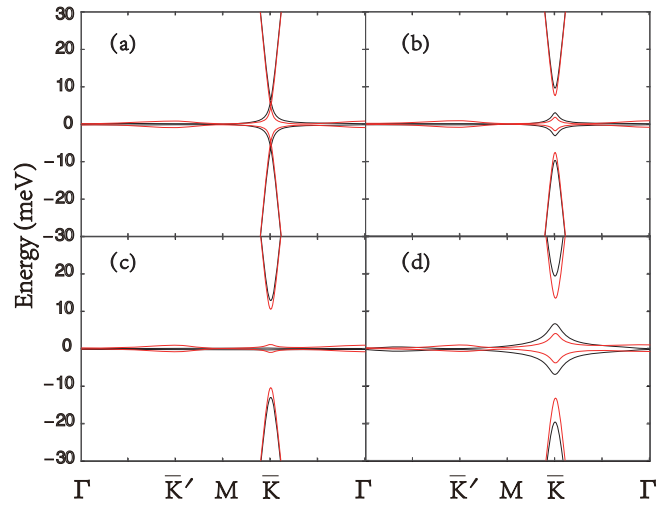

FIG. 3. Spectra of the flat bands with lateral shift $d_x = 0.06a$ and $d_y = 0$ in the chiral limit $w_{\mathrm{AA}} = 0$ (black line) and in the nonchiral limit $w_{\mathrm{AA}} = 6$ meV (red line). The zero energy is set at the band center. The in-plane magnetic field is set as (a) $B = 0$, (b) $B = 5$ T, (c) $B = 7.5$ T, (d) $B = 10$ T.

given as

$$\mathcal{H}_K^c(\boldsymbol{k}) = v_{\mathrm{D}}\begin{pmatrix} 0 & D_{\boldsymbol{k}}(\boldsymbol{r}) \\ D_{\boldsymbol{k}}^*(-\boldsymbol{r}) & 0 \end{pmatrix}, \tag{5}$$

in which

$$D_{\boldsymbol{k}}(\boldsymbol{r}) = \begin{pmatrix} k_x - ik_y & \alpha U(\boldsymbol{r}) & A_x - iA_y \\ \alpha U(-\boldsymbol{r}) & k_x - ik_y & \alpha V(-\boldsymbol{r}) \\ A_x - iA_y & \alpha V(\boldsymbol{r}) & k_x - ik_y \end{pmatrix}, \tag{6}$$

where $\alpha = w_{\mathrm{AB}}/v_{\mathrm{D}}$, $U(\boldsymbol{r}) = e^{-i\boldsymbol{q}_1\cdot\boldsymbol{r}} + \cos(\boldsymbol{G}_2\cdot\boldsymbol{d}/2)e^{-i\phi}e^{-i\boldsymbol{q}_2\cdot\boldsymbol{r}} + \cos(\boldsymbol{G}_3\cdot\boldsymbol{d}/2)e^{i\phi}e^{-i\boldsymbol{q}_3\cdot\boldsymbol{r}}$, and $V(\boldsymbol{r}) = \sin(\boldsymbol{G}_2\cdot\boldsymbol{d}/2)e^{-i\phi}e^{-i\boldsymbol{q}_2\cdot\boldsymbol{r}} + \sin(\boldsymbol{G}_3\cdot\boldsymbol{d}/2)e^{i\phi}e^{-i\boldsymbol{q}_3\cdot\boldsymbol{r}}$.

The chirally symmetric Hamiltonian leads to the particle-hole symmetry with respect to $\varepsilon = 0$. In the limit of $\boldsymbol{A} = 0$ and $\boldsymbol{d} = 0$, the lowest band becomes absolutely flat at the magic angle. In this limit, the effective twisted bilayer part is decoupled from the effective single layer part, hence the wave function of the flat band is reminiscent of that of MATBG and satisfies the equation $D_{\boldsymbol{k}}(\boldsymbol{r})\Phi_{\boldsymbol{k}}(\boldsymbol{r}) = 0$, with the wave function taking an exact representation

$$\Phi_{\boldsymbol{k}}(\boldsymbol{r}) = \begin{pmatrix} \psi_1(\boldsymbol{r}) \\ \psi_2(\boldsymbol{r}) \\ 0 \end{pmatrix} = f_{\boldsymbol{k}}(z)\Phi_{\overline{K}}(\boldsymbol{r}), \tag{7}$$

where $\Phi_{\overline{K}}(\boldsymbol{r})$ is the zero-mode wave function at the Dirac point $\overline{K}$ and $f_{\boldsymbol{k}}(z)$ can be interpreted as a quantum Hall wave function of the lowest Landau level [36]. When $\boldsymbol{A}$ and $\boldsymbol{d}$ are both turned on, we also find super flat bands for certain conditions. As the lateral shift is small, i.e., $T'(\boldsymbol{r}) \approx T(\boldsymbol{r})$, we use the ansatz that the wave function is almost the same as in the $\boldsymbol{A} = 0, \boldsymbol{d} = 0$ case. To make the equation $D_{\boldsymbol{k}}(\boldsymbol{r})\Phi_{\boldsymbol{k}}(\boldsymbol{r}) = 0$ approximately correct again, one need to make sure that

$$(A_x - iA_y)\psi_1(\boldsymbol{r}) + \alpha V(\boldsymbol{r})\psi_2(\boldsymbol{r}) \approx 0. \tag{8}$$

In other words, if the in-plane magnetic field and the lateral shift meet the above condition, one can find the perfect flat bands again. In Fig. 3(c), we set $d_x = 0.06a$, $d_y = 0$, and $B = 7.5$ T, and confirm that the bandwidth of the lowest bands is almost zero.

By common sense, it is believed that the presence of a magnetic field breaks superconductivity and causes a decrease in the superconducting transition temperature with increasing magnetic field strength. However, in Figs. 3(a)–3(c), we observe that the width of the lowest-energy bands continuously narrows as the magnetic field increases. This gives us an insight: with the assistance of lateral shifts, the increase in magnetic field leads to a reduction in the bandwidth, which in turn results in an increase in the DOS. At certain parameters, this increase in the DOS manifests as a peak. One can expect that this peak in the DOS leads to an increase in the transition temperature of superconductivity. This phenomenon, where superconductivity is enhanced with increasing magnetic field strength, is really intriguing.

As an idealized model, it captures the key features of the band structures changing as a function of in-plane magnetic field in the chiral limit. In reality, the parameter w_{AA} may influences the band structures, and the results may vary when w_{AA} is nonzero. In Fig. 3, we compare the band structures for $w_{\mathrm{AA}} = 0$ and $w_{\mathrm{AA}} = 6$ meV. In the vicinity of the $\overline{K}$ point, the overall trend of the band structures change with the magnetic field is consistent in both cases. Near the Γ point, the nonzero w_{AA} term introduces a finite band widening but does not alter with in-plane magnetic field. Therefore, we find that in both cases the DOS is increased at certain values of in-plane magnetic field, and the calculations in the chiral limit are still reliable.

B. Enhanced superconductivity with in-plane magnetic Field

The low-energy bands of MATTG manifest a large DOS similar to MATBG, which opens up an avenue for exploring interesting many-body phenomena such as superconductivity. We consider a BCS type interaction mediated by the in-plane acoustic phonons, which is given as

$$\mathcal{H}_{\mathrm{BCS}} = -g_0\sum_{l\sigma}\int d\boldsymbol{r}\psi_{+l\sigma}^\dagger(\boldsymbol{r})\psi_{-l\sigma}^\dagger(\boldsymbol{r})\psi_{-l\sigma}(\boldsymbol{r})\psi_{+l\sigma}(\boldsymbol{r}), \tag{9}$$

where $\pm$, l, and σ are valley, layer, and sublattice indices, respectively. The coupling constant g_0 denotes the phonon-mediated effective attraction between the electrons and is given by $g_0 = 320$ meV nm^2 [38]. This choice yields the critical temperature approximately 2 K in the absence of in-plane magnetic field and lateral shifts, comparable with experimental results [28,40,41].

We focus on the two flat bands near the charge neutrality point, which exhibit the large DOS and van Hove singularity, making them suitable for investigating superconductivity. Although these bands are connected to higher-energy bands in the absence of a in-plane magnetic field, their contribution to superconductivity is significant. When the Fermi energy falls within these bands, the projected BCS pairing interaction is given by

$$\mathcal{H}'_{\mathrm{BCS}} = \frac{-1}{\mathcal{A}}\sum_{nn'\boldsymbol{k}\boldsymbol{k}'} g_{\boldsymbol{k}\boldsymbol{k}'}^{nn'} c_{+n}^\dagger(\boldsymbol{k})c_{-n}^\dagger(-\boldsymbol{k})c_{-n'}(-\boldsymbol{k}')c_{+n'}(\boldsymbol{k}'), \tag{10}$$

with

$$g_{\boldsymbol{k}\boldsymbol{k}'}^{nn'} = g_0\sum_{l\sigma}\phi_{+nl\sigma}^*(\boldsymbol{k})\phi_{-nl\sigma}^*(-\boldsymbol{k})\phi_{+n'l\sigma}(\boldsymbol{k}')\phi_{-n'l\sigma}(-\boldsymbol{k}'), \tag{11}$$

where $\mathcal{A}$ is the area of the system and the Cooper pairs are confined within the same band. The term $\phi_{\pm nl\sigma}(\boldsymbol{k})$ represents the component of the wave function of the nth energy band at momentum $\boldsymbol{k}$, with respect to the indices l and σ. A large in-plane magnetic field breaks the time-reversal symmetry and suppresses the singlet pairing through the Zeeman term, making spin-triplet pairing the only possibility. Hence, in the model considered in this study, we assume that the system is spin polarized.

In the mean field approximation [42], the pairing function becomes

$$\Delta^n(\boldsymbol{k}) = \frac{1}{\mathcal{A}}\sum_{n'\boldsymbol{k}'} g_{\boldsymbol{k}\boldsymbol{k}'}^{nn'}\langle c_{-n'}(-\boldsymbol{k}')c_{+n'}(\boldsymbol{k}')\rangle. \tag{12}$$

Near the transition temperature, we derive the linearized gap equation as

$$\Delta^n(\boldsymbol{k}) = \sum_{n'\boldsymbol{k}'}\chi_{\boldsymbol{k}\boldsymbol{k}'}^{nn'}\Delta^{n'}(\boldsymbol{k}'), \tag{13}$$

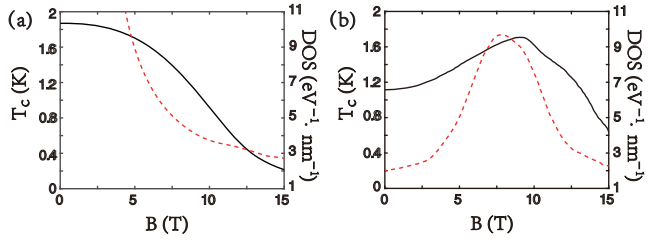

FIG. 4. Superconducting transition temperature T_c versus in-plane magnetic field B under different parameters. In all the figures, we set the parameter $d_y = 0$. d_x is set as (a) $d_x = 0$, (b) $d_x = 0.06a$. The solid black lines represent T_c, while the dashed red lines represent the corresponding DOS. It is observed that the maximum position of T_c always coincides with the peak position of DOS.

in which

$$\chi_{\boldsymbol{k}\boldsymbol{k}'}^{nn'} = \frac{g_{\boldsymbol{k}\boldsymbol{k}'}^{nn'}}{\mathcal{A}} \frac{1 - f[\varepsilon_+^{n'}(\boldsymbol{k}')] - f[\varepsilon_-^{n'}(-\boldsymbol{k}')]}{\varepsilon_+^{n'}(\boldsymbol{k}') + \varepsilon_-^{n'}(-\boldsymbol{k}') - 2E_F}, \tag{14}$$

where $\varepsilon_\pm^n(\boldsymbol{k})$ is the energy dispersion of the flat band in valley $\pm$ and $f(E)$ represents the Fermi distribution function. Notice that Eq. (13) is a self-consistent equation, where the transition temperature T_c can be determined by finding the highest temperature such that the largest value of χ equals 1.

At a fixed filling level $\nu = -2.4$, we numerically obtain T_c as a function of in-plane magnetic field B in Fig. 4. We find that the largest T_c coincides with the maximum DOS. In Fig. 4(a), at $\boldsymbol{d} = 0$, the highest T_c occurs at $B = 0$ because the system possesses a completely flat energy band, resulting in the maximum DOS at this point. In Fig. 4(b), when $\boldsymbol{d}$ is nonzero an appropriate in-plane magnetic field can reduce the bandwidth of the flat band, as described in Fig. 3(c). Consequently, the peak of the DOS is observed near $B = 7.5$ T, coinciding with the peak in T_c of $B = 8$ T. These two figures demonstrate the significant influence of the DOS on the superconducting temperature, as discussed in the BCS theory.

C. Reentrant superconductivity

The electric displacement field induced by gates plays a crucial role in the observed superconductivity [28], the physics of the superconductivity is also closely related to the strength of the electric displacement field. The electric displacement field enters the Hamiltonian (4) through an on-site potential of $(V_0, 0, -V_0)$ on layers 1, 2, and 3, respectively. In the presence of the electric displacement field, T_c drops rapidly with the increase of B. This is caused by the fact that the electric displacement field destroys the $\mathcal{C}_2\mathcal{M}_h$ symmetry which is preserved by lateral shifts and in-plane magnetic field [35,38]. The $\mathcal{C}_2\mathcal{M}_h$ symmetry makes sure that the energy bands satisfy $\varepsilon_+^n(\boldsymbol{k}) = \varepsilon_-^n(-\boldsymbol{k})$ even in the presence of B, suggesting a perfect intervalley Fermi surface nesting. The electric displacement field, however, lifts the pairing degeneracy and leads to a reduction of T_c [38].

In the case of $\boldsymbol{d} = 0$ as shown in Fig. 5(a), the electric displacement field leads to a rapid decrease in T_c due to both the symmetry breaking induced energy mismatch of the pairing electrons and the decrease of the DOS. In the case of $d_x = 0.06a$ and $d_y = 0$ as shown in Fig. 5(b), however, we find

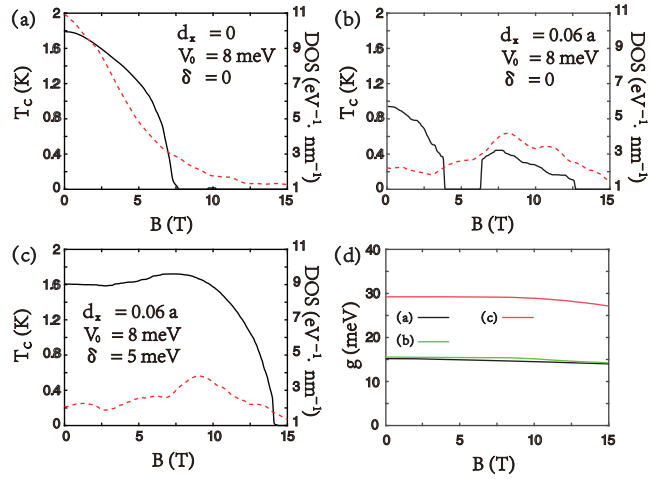

FIG. 5. Comparative dependence of T_c on B in two scenarios: (a) and (b) absence of sublattice polarization, and (c) presence of sublattice polarization under a finite electric displacement field. In all the figures, we set the parameter $d_y = 0$. The solid black lines represent T_c, while the dashed red lines represent the corresponding DOS. In certain specific parameter regimes, such as in (b), there exists reentrant superconductivity. (d) Average interaction under the parameters depicted in (a), (b), and (c).

that the reentrance of superconductivity occurs. Initially T_c decreases rapidly with increasing B until it reaches zero. However, as B continues to increase, T_c becomes nonzero again, corresponding to the experimentally observed reentrant superconductivity [28]. By calculating the DOS, we verify that the region of reentrant superconductivity coincides precisely with the peak in the DOS. The appearance of the peak in the DOS indicates that the band is flattened by the increase of B. Even though both superconductivity and correlated insulating behavior are strongest near the extremely flat band condition, superconductivity is more favored away from integer fillings. Therefore, we believe that the phenomena of reentrant superconductivity is a competition between the decrease in T_c caused by the electric displacement field and the increase in T_c due to the band flattening. In the region where B is not too large, since the DOS does not show significant changes with increasing B, the dominant effect is the decrease in T_c caused by the electric displacement field, resulting in a rapid decrease of T_c to zero. However, as B continues to increase and the DOS significantly rises, T_c starts to increase again, leading to the occurrence of the reentrant superconducting phase.

Another factor influencing the variation of T_c is the sublattice polarization. When a sublattice polarization term $\mathrm{Diag}(\delta_1\sigma_z, 0, \delta_3\sigma_z)$ is added in Hamiltonian (4), the lowest bands are separated from each other. In Fig. 5(c), we include the sublattice polarization $\delta_{1,3} = 5$ meV. We find that, when the sublattice polarization is turned on, the electric displacement field loses its control over T_c. In this case, the variation trend of T_c is synchronized with the change of the DOS again. Interestingly, the sublattice polarization also breaks the $\mathcal{C}_2\mathcal{M}_h$ symmetry [38]. Therefore, the breaking of $\mathcal{C}_2\mathcal{M}_h$ symmetry is not the fundamental reason for the decrease in T_c.

To unravel this puzzle, we further investigate the variation of the average attractive interaction with magnetic field under

different parameter settings. We define the average attractive interaction as

$$\bar{g} \equiv \frac{1}{4N^2} \sum_{nn'\boldsymbol{k}\boldsymbol{k}'} g^{nn'}_{\boldsymbol{k}\boldsymbol{k}'}, \tag{15}$$

where N represents the number of $\boldsymbol{k}$ points sampled in the numerical calculations. The magnitude of $\bar{g}$ is directly related to the value of T_c. In Fig. 5(d), we calculate the values of $\bar{g}$ under different parameter settings and find that, when sublattice polarization term is present, $\bar{g}$ is nearly twice as large compared to the one when sublattice polarization term is absent. This result indicates that superconductivity exhibits remarkable robustness when the sublattice polarization term exists. Consequently, the sublattice polarization term stabilizes superconductivity instead of breaking it.

Sublattice polarization can be induced if a graphene layer is perfectly aligned with a hBN substrate. In MATBG, aligned samples show no evidence for superconductivity, in contrast with unaligned samples [43]. We attribute this phenomenon to the breaking of $\mathcal{C}_2$ symmetry by the sublattice polarization. It is worth noticing that in MATBG the electron states in the two valleys can be transformed to each other through $\mathcal{T}$ and $\mathcal{C}_2$ symmetries. The breaking of $\mathcal{C}_2$ symmetry will introduce valley polarization caused by the Coulomb interaction which has been widely explored [44,45]. The valley polarization breaks the degeneracy of electron pairs that combine to form Cooper-pair bound states, and then extinguish the superconductivity. However, in the MATTG case, there are three intervalley symmetry operations, i.e., $\mathcal{T}$, $\mathcal{T}\mathcal{M}_h$, and $\mathcal{C}_2\mathcal{M}_h$. When the sublattice polarization, lateral shift, and in-plane magnetic field are taken into account, each one alone conserves two symmetries. Due to the protection of multiple symmetries, valley polarization is not easy to form, just like the unaligned MATBG, therefore the superconductivity is more robust. In experiments, it is not quite common to make the MATTG perfectly aligned to the hBN substrate. Certainly, it will be an interesting topic for experimental investigations.

IV. DISCUSSION AND CONCLUSIONS

The addition of more layers can typically convert the system from two-dimensional to three-dimensional, and may diminish the impact of the large density of states originating from the flat bands. However, by limiting the stack to just a few layers and employing a suitable sequence of twist angles, one can still observe the persistence of flat band behavior in the low-energy regime. This is particularly evident in MATTG, where the mirror symmetry and the lateral shift enhance the resilience of flat bands to perturbations from in-plane magnetic fields. MATTG provides an excellent platform for studying correlated physics.

We have investigated the influence of different external factors on superconductivity in the MATTG system, including an in-plane magnetic field, small lateral shift of an outer layer, electric displacement fields induced by gates, and sublattice polarization. We have found that these factors have distinct effects on superconductivity. Surprisingly, the most significant factor is small lateral shifts. Their importance lies in the fact that their combined effect with magnetic fields leads to an enhanced DOS in the flat bands. Within certain specific parameter ranges, perfect flat bands can emerge. With the enhancement of the DOS, T_c exhibits a peak near the DOS peak, demonstrating an anomalous superconducting behavior that strengthens with the increase of magnetic field strength.

In this work, we have shown that lateral shifts are essential to explain the reentrance of superconductivity in MATTG. The direct evidence is that in the presence of lateral shifts, the increase of B field first flattens the lowest bands then widens them. There is a special value of B field that makes the lowest bands almost perfectly flat, and this value of B field strongly depends on lateral shifts which should be different between samples. However, the critical B field in experiment represents the point where the B field breaks the coherence of Cooper pairs, and then the superconductivity is lost. In the BCS framework, our calculations have verified that the reentrance of superconductivity mainly comes from the energy rematch of electrons forming Cooper pairs during the band flattening. Lateral shifts facilitate the enhancement of the DOS, which helps to enlarge the critical temperature in the superconducting reentrance region, but does not affect the critical B field. Therefore, the critical B field is relatively consistent between devices.

In addition, the induction of an electric displacement field breaks the $\mathcal{C}_2\mathcal{M}_h$ symmetry. Cooper pairs experience energy splitting due to the presence of the electric displacement field, leading to a decrease in the pairing temperature. Our calculations have confirmed these results. However, we have found that the breaking of the $\mathcal{C}_2\mathcal{M}_h$ symmetry does not necessarily directly lead to a decrease in T_c, as is the case with the sublattice polarization term. We have observed that the presence of the sublattice polarization term enhances the strength of the effective interaction projected onto the flat bands. Despite the breaking of the $\mathcal{C}_2\mathcal{M}_h$ symmetry, the stronger attractive interaction also leads to an increase in T_c. Therefore, in MATTG, the different external fields exhibit competitive effects. For example, the increased DOS resulting from lateral shifts leads to an increase in T_c, while the breaking of the $\mathcal{C}_2\mathcal{M}_h$ symmetry by the electric displacement field leads to a decrease in T_c. The interplay between these two mechanisms can result in the occurrence of reentrant superconductivity under specific parameter settings. Similarly, the electric displacement field and sublattice polarization, both breaking the $\mathcal{C}_2\mathcal{M}_h$ symmetry, have opposite effects on T_c. The inclusion of the sublattice polarization term actually stabilizes T_c.

In summary, the study of twisted multilayer graphene systems, particularly MATTG, has opened up exciting new possibilities for exploring superconductivity and other exotic phenomena in strongly correlated electron systems. The experimental observation of enhanced robustness of superconductivity in the MATTG system compared to the MATBG system can be attributed to the strengthening effect of external fields on T_c. Factors that elevate the transition temperature T_c include small lateral shifts and sublattice polarization, while external fields that weaken T_c include (but are not limited to) the electric displacement field. Our findings suggest that the coexistence of a small lateral shift between the outer layers and an electric displacement field is crucial for achieving the reentrant superconductivity in MATTG. Our discovery of the quasiflat bands' reemergence in MATTG with small lateral shifts and large in-plane magnetic fields, leading to a

peak value of the DOS and enhancing the superconducting transition temperature, is particularly intriguing. Furthermore, a sublattice polarization term is valuable for stabilizing the superconductivity instead of destroying it. Our work provides valuable insights into the behavior of twisted multilayer graphene systems and highlights the importance of external fields and small lateral shifts for tuning their electronic properties.

It was recently brought to our attention that exact results in the flat band limit have been discussed comprehensively [46,47]. The DOS enhancement caused by the band flattening is also found to be important within the BCS theory. In the flat band limit, however, other researches have confirmed that the critical temperature is believed to follow Berezinskii-Kosterlitz-Thouless behavior determined by the superfluid weight or quantum geometry related to the Fubini-Study metric [48], which could have an important effect in addition to the DOS. These results are important avenues of research and deserve to be studied further in the future.

ACKNOWLEDGMENTS

This work was supported by the National Natural Science Foundation of China (Grants No. 12074156, No. 12104232, and No. 22075068) and the Fundamental Research Funds for the Central Universities (Grant No. B230201042).

[1] Y. Cao, V. Fatemi, A. Demir, S. Fang, S. L. Tomarken, J. Y. Luo, J. D. Sanchez-Yamagishi, K. Watanabe, T. Taniguchi, E. Kaxiras, R. C. Ashoori, and P. Jarillo-Herrero, Nature (London) **556**, 80 (2018).
[2] Y. Cao, V. Fatemi, S. Fang, K. Watanabe, T. Taniguchi, E. Kaxiras, and P. Jarillo-Herrero, Nature (London) **556**, 43 (2018).
[3] M. Yankowitz, S. Chen, H. Polshyn, Y. Zhang, K. Watanabe, T. Taniguchi, D. Graf, A. F. Young, and C. R. Dean, Science **363**, 1059 (2019).
[4] X. Lu, P. Stepanov, W. Yang, M. Xie, M. A. Aamir, I. Das, C. Urgell, K. Watanabe, T. Taniguchi, G. Zhang, A. Bachtold, A. H. MacDonald, and D. K. Efetov, Nature (London) **574**, 653 (2019).
[5] C. Xu and L. Balents, Phys. Rev. Lett. **121**, 087001 (2018).
[6] H. C. Po, L. Zou, A. Vishwanath, and T. Senthil, Phys. Rev. X **8**, 031089 (2018).
[7] H. Isobe, N. F. Q. Yuan, and L. Fu, Phys. Rev. X **8**, 041041 (2018).
[8] C.-C. Liu, L.-D. Zhang, W.-Q. Chen, and F. Yang, Phys. Rev. Lett. **121**, 217001 (2018).
[9] D. M. Kennes, J. Lischner, and C. Karrasch, Phys. Rev. B **98**, 241407(R) (2018).
[10] H. Guo, X. Zhu, S. Feng, and R. T. Scalettar, Phys. Rev. B **97**, 235453 (2018).
[11] Y.-Z. You and A. Vishwanath, npj Quantum Mater. **4**, 16 (2019).
[12] J. González and T. Stauber, Phys. Rev. Lett. **122**, 026801 (2019).
[13] B. Roy and V. Juričić, Phys. Rev. B **99**, 121407(R) (2019).
[14] S. Ray, J. Jung, and T. Das, Phys. Rev. B **99**, 134515 (2019).
[15] T. Cea and F. Guinea, Proc. Natl. Acad. Sci. USA **118**, e2107874118 (2021).
[16] Y. W. Choi and H. J. Choi, Phys. Rev. B **98**, 241412(R) (2018).
[17] F. Wu, A. H. MacDonald, and I. Martin, Phys. Rev. Lett. **121**, 257001 (2018).
[18] B. Lian, Z. Wang, and B. A. Bernevig, Phys. Rev. Lett. **122**, 257002 (2019).
[19] M. Angeli, E. Tosatti, and M. Fabrizio, Phys. Rev. X **9**, 041010 (2019).
[20] F. Wu, E. Hwang, and S. Das Sarma, Phys. Rev. B **99**, 165112 (2019).
[21] C. Lewandowski, S. Nadj-Perge, and D. Chowdhury, npj Quantum Mater. **6**, 82 (2021).
[22] J. Cao, F. Qi, Y. Xiang, and G. Jin, Phys. Rev. B **106**, 115436 (2022).
[23] M. Koshino, Phys. Rev. B **99**, 235406 (2019).
[24] J. Liu, Z. Ma, J. Gao, and X. Dai, Phys. Rev. X **9**, 031021 (2019).
[25] E. Khalaf, A. J. Kruchkov, G. Tarnopolsky, and A. Vishwanath, Phys. Rev. B **100**, 085109 (2019).
[26] G. A. Tritsaris, S. Carr, Z. Zhu, Y. Xie, S. B. Torrisi, J. Tang, M. Mattheakis, D. Larson, and E. Kaxiras, 2D Mater. **7**, 035028 (2020).
[27] Z. Ma, S. Li, Y.-W. Zheng, M.-M. Xiao, H. Jiang, J.-H. Gao, and X. C. Xie, Sci. Bull. **66**, 18 (2021).
[28] Y. Cao, J. M. Park, K. Watanabe, T. Taniguchi, and P. Jarillo-Herrero, Nature (London) **595**, 526 (2021).
[29] D. Guerci, P. Simon, and C. Mora, Phys. Rev. Res. **4**, L012013 (2022).
[30] A. Fischer, Z. A. H. Goodwin, A. A. Mostofi, J. Lischner, D. M. Kennes, and L. Klebl, npj Quantum Mater. **7**, 5 (2022).
[31] I. A. Assi, J. P. F. LeBlanc, M. Rodriguez-Vega, H. Bahlouli, and M. Vogl, Phys. Rev. B **104**, 195429 (2021).
[32] C. Mora, N. Regnault, and B. A. Bernevig, Phys. Rev. Lett. **123**, 026402 (2019).
[33] S. Carr, C. Li, Z. Zhu, E. Kaxiras, S. Sachdev, and A. J. Kruchkov, Nano Lett. **20**, 3030 (2020).
[34] Z. Zhu, S. Carr, D. Massatt, M. Luskin, and E. Kaxiras, Phys. Rev. Lett. **125**, 116404 (2020).
[35] C. Lei, L. Linhart, W. Qin, F. Libisch, and A. H. MacDonald, Phys. Rev. B **104**, 035139 (2021).
[36] G. Tarnopolsky, A. J. Kruchkov, and A. Vishwanath, Phys. Rev. Lett. **122**, 106405 (2019).
[37] N. Bultinck, E. Khalaf, S. Liu, S. Chatterjee, A. Vishwanath, and M. P. Zaletel, Phys. Rev. X **10**, 031034 (2020).
[38] W. Qin and A. H. MacDonald, Phys. Rev. Lett. **127**, 097001 (2021).
[39] R. Bistritzer and A. H. MacDonald, Proc. Natl. Acad. Sci. USA **108**, 12233 (2011).
[40] J. M. Park, Y. Cao, K. Watanabe, T. Taniguchi, and P. Jarillo-Herrero, Nature (London) **590**, 249 (2021).
[41] Z. Hao, A. M. Zimmerman, P. Ledwith, E. Khalaf, D. H. Najafabadi, K. Watanabe, T. Taniguchi, A. Vishwanath, and P. Kim, Science **371**, 1133 (2021).

[42] Y.-Z. Chou, F. Wu, J. D. Sau, and S. Das Sarma, Phys. Rev. Lett. **127**, 187001 (2021).

[43] M. Oh, K. P. Nuckolls, D. Wong, R. L. Lee, X. Liu, K. Watanabe, T. Taniguchi, and A. Yazdani, Nature (London) **600**, 240 (2021).

[44] M. Serlin, C. L. Tschirhart, H. Polshyn, Y. Zhang, J. Zhu, K. Watanabe, T. Taniguchi, L. Balents, and A. F. Young, Science **367**, 900 (2020).

[45] Y.-H. Zhang, D. Mao, and T. Senthil, Phys. Rev. Res. **1**, 033126 (2019).

[46] X. Zhang, K. Sun, H. Li, G. Pan, and Z. Y. Meng, Phys. Rev. B **106**, 184517 (2022).

[47] J. H.-Arbeitman, A. Chew, K.-E. Huhtinen, P. Törmä, and B. A. Bernevig, arXiv:2209.00007.

[48] S. Peotta and P. Törmä, Nat. Commun. **6**, 8944 (2015).